Supporting Information

Negative Photoconductivity Photodetector based on two-dimesional Nb_3Cl_8

Bom Lee[a,†], Xiaojie Zhang[a†], Jinsu Kang [a], Byung Joo Jeong[a], Sooheon Cho[a], Kyung Hwan choi[b], Jiho Jeon[b], Sang Hoon Lee[a], Dahoon Kim[a], Yeong Hyeop Kim[a], Ji-Hee Kim[c,], Hak Ki Yu[d,*], and Jae-Young Choi[a,b,*]*

[a]School of Advanced Materials Science and Engineering, Sungkyunkwan University, Suwon 16419, Republic of Korea

[b]SKKU Advanced Institute of Nanotechnology (SAINT), Sungkyunkwan University, Suwon 16419, Republic of Korea

[c]Department of Physics, Pusan National University, Busan 46241, Republic of Korea.

[d]Department of Materials Science and Engineering & Department of Energy Systems Research, Ajou University, Suwon 16499, Republic of Korea.

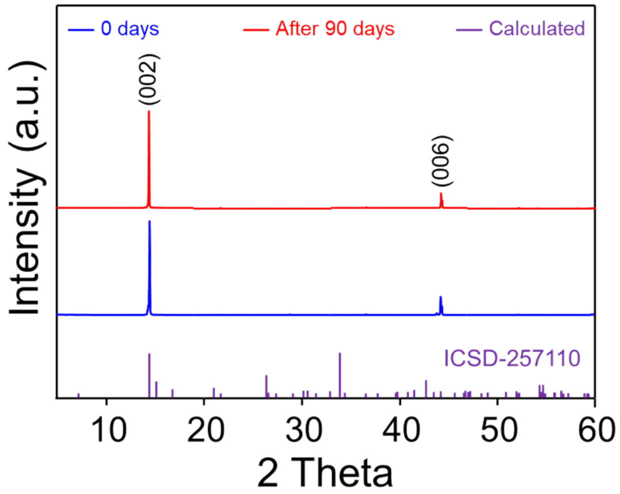

Fig. S1. Materials stability characteristic of Nb_3Cl_8

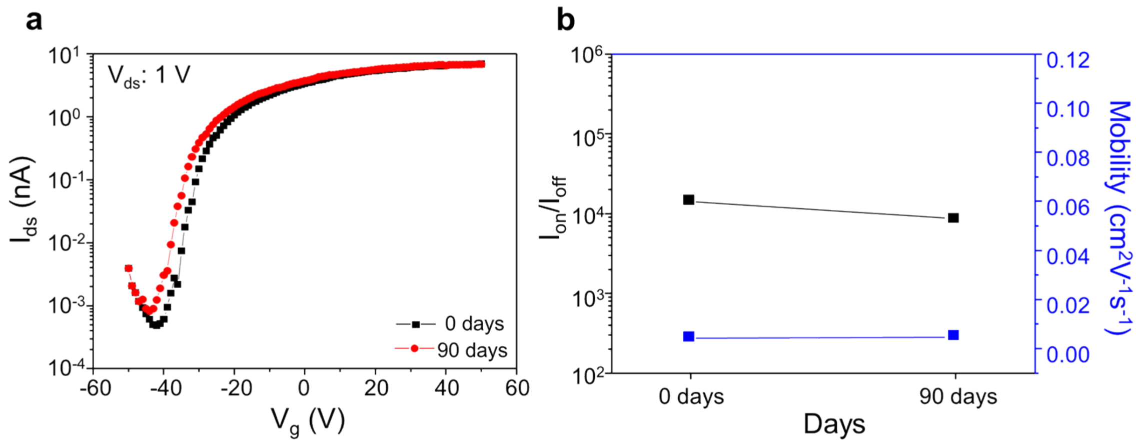

Fig. S2. Device stability characteristic of 8.72 nm thick Nb_3Cl_8 FET

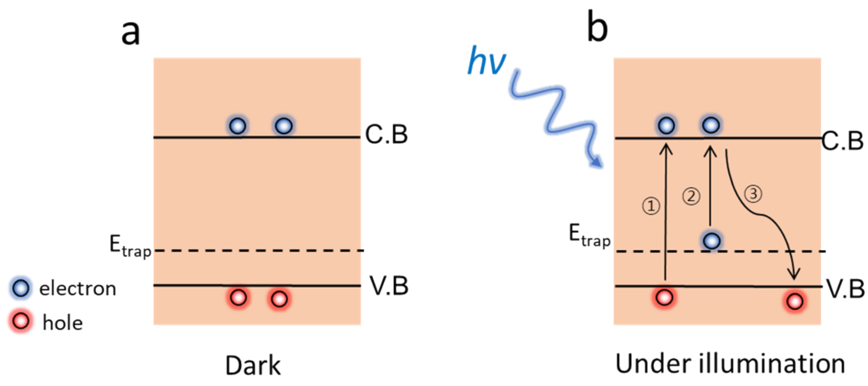

Fig. S3. Energy band diagram showing the photoresponse process within the Nb_3Cl_8

In process ①, electrons in the valence band (E_v) absorb photon energy and are excited to the conduction band (E_c), generating electron-hole pairs and increasing the hole concentration. This represents the conventional photoexcitation mechanism. Concurrently, process ② involves the excitation of electrons from trap levels (E_{trap}) within the bandgap to the conduction band. However, the key to the observed negative photoconductivity lies in process ③, where photo-induced electrons recombine with holes in the valence band through these trap states, effectively reducing the overall hole concentration. This recombination process, facilitated by the presence of trap levels, is the primary driver of the decrease in conductivity under illumination, leading to the NPC phenomenon in Nb_3Cl_8.

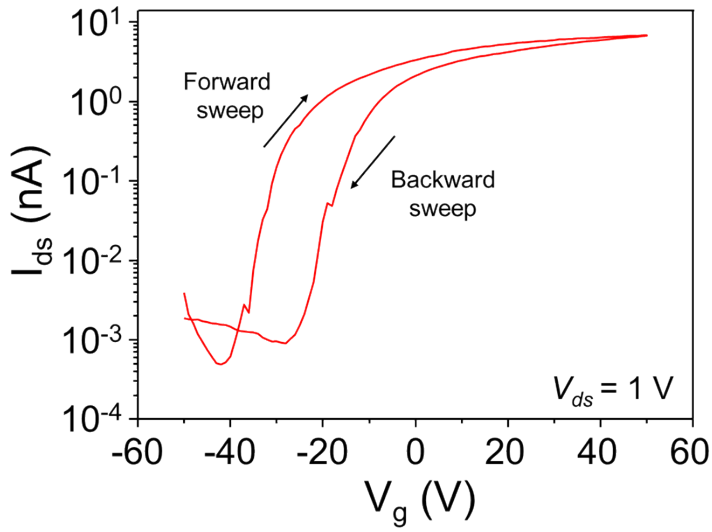

Fig. S4. Hysteresis loop in the transfer characteristics of Nb_3Cl_8

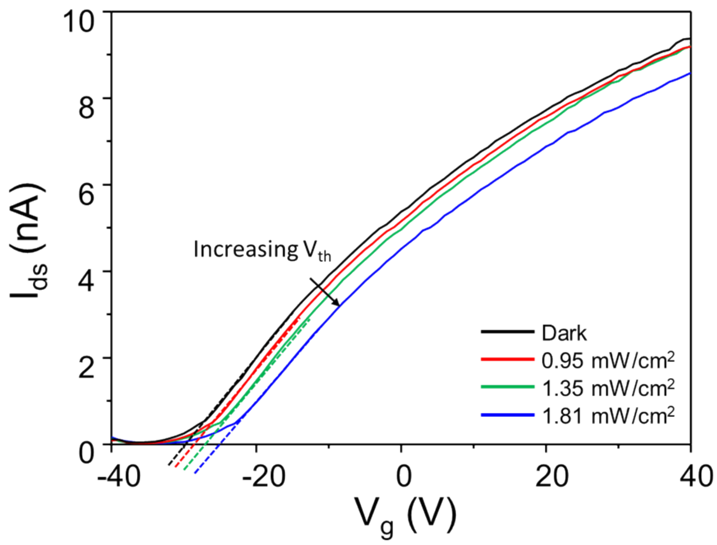

Fig. S5. Transfer characteristics (I_{ds}-V_g) of Nb_3Cl_8 nanosheets, obtained by sweeping the gate voltage from −40 to 40 V under dark and ligh at fixed V_{ds} of 1 V.

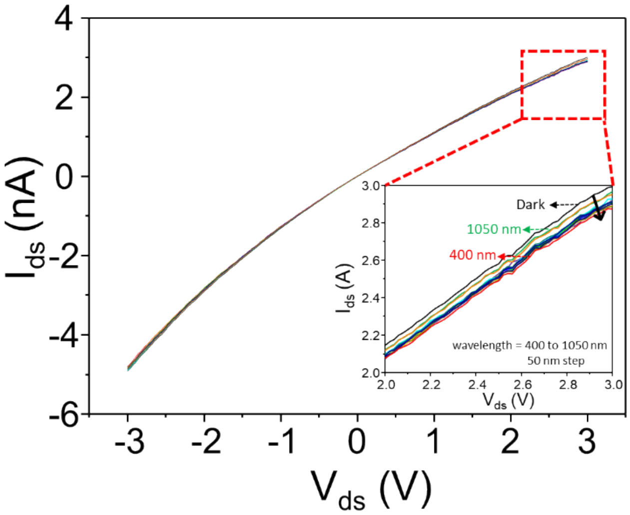

Fig. S6. I_{ds}-V_{ds} curve of the Nb_3Cl_8 in the dark mode and under light illumination with different wavelength from 400 to 1050 nm

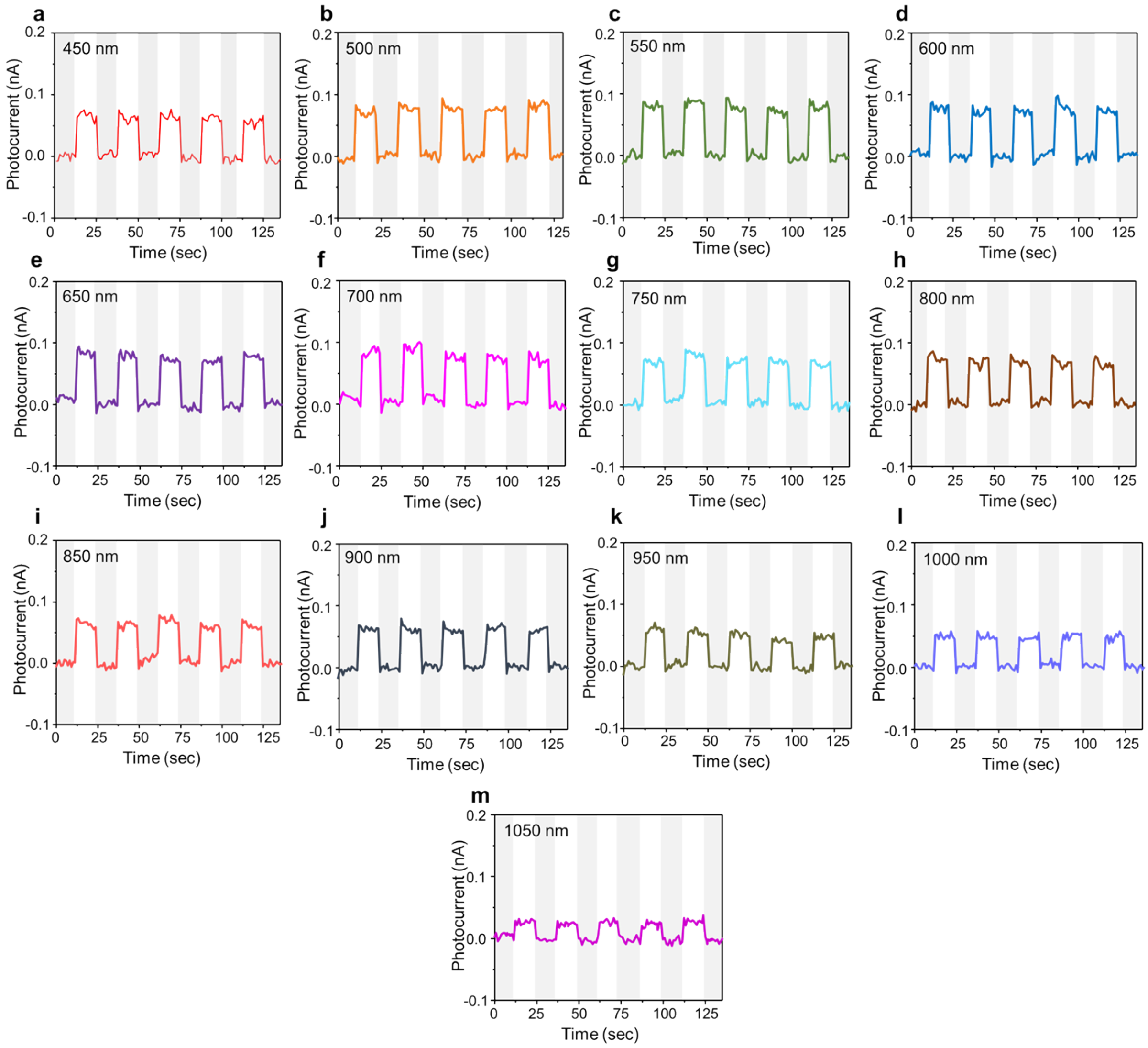

Fig. S7. Time-resolved photo response of the Nb_3Cl_8 at V_{ds} = 3 V under different wavelength ranges (450-1050 nm) with a power density of 1.54 mW/cm^2.

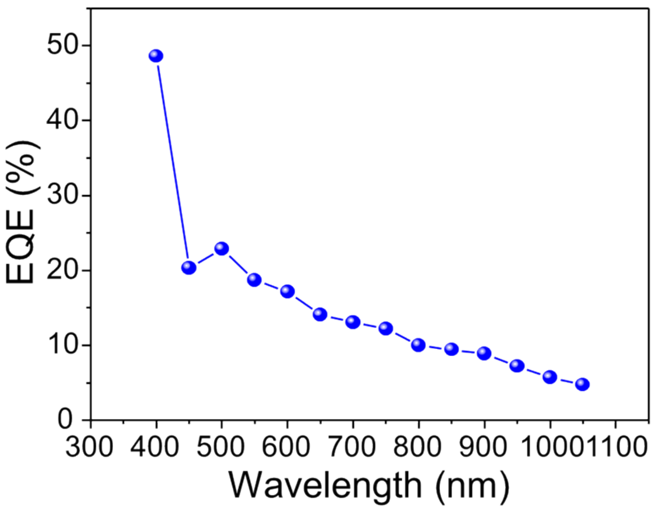

Fig. S8. Wavelength dependent EQE at V_{ds} = 3 V and power density = 1.54 mW/cm^2.

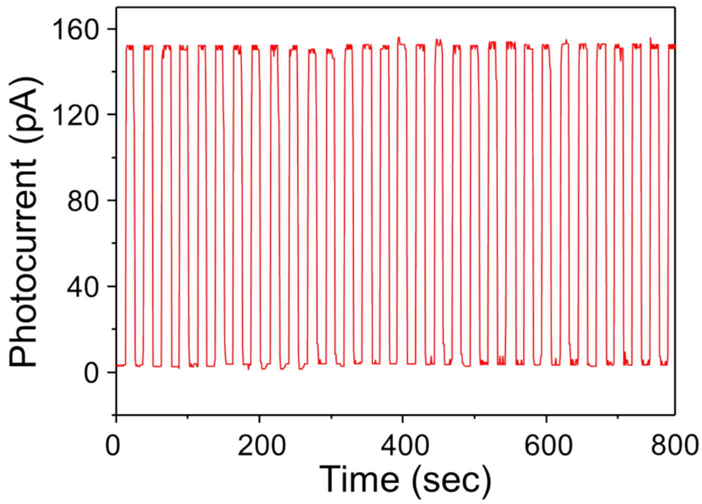

Fig. S9. Photocurrent stability characteristic of 8.72 nm thick Nb_3Cl_8 FET

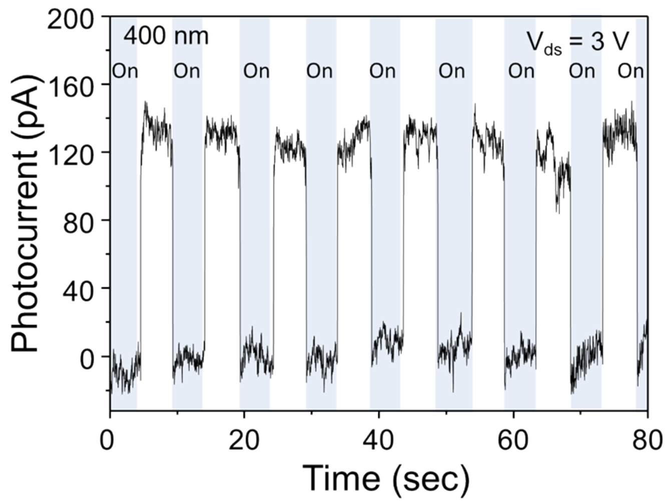

Fig. S10. Time-resolved photoresponse in vacuum condition at V_{ds} = 3 V and power density = 1.54 mW/c

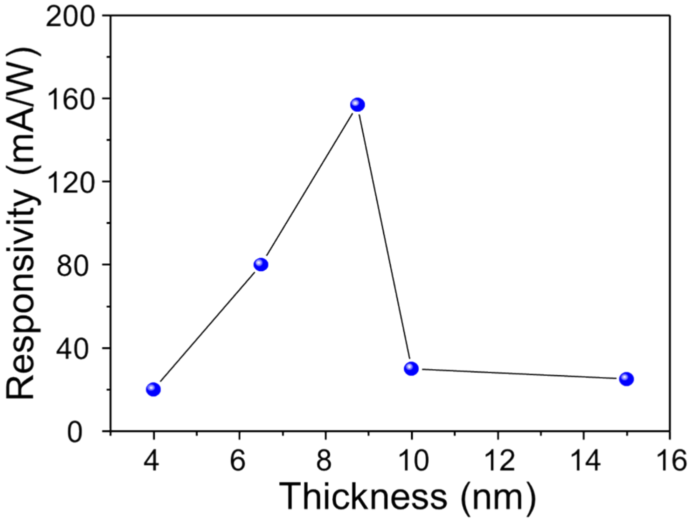

Fig S11. Thickness-dependent responsivity of Nb_3Cl_8 nanoflakes.

Table. S1. Comparison table of key parameters of 2D NPC

Material	Bias Voltage (V)	Wavelength (nm)	Source	Responsivity (mA/W)	Detectivity (Jones)	Response Time rise/decay (ms/ms)	Ref.
$MoTe_2$/hBN/graphene	-	635	light	~500	~1.6×10^{12}	~3	[1]
WTe_2/GaAs	0.6	1064	laser	271	9.18×10^{11}	-	[2]
InAs	0.1	700	laser	1.231×10^{6}	5.46×10^{10}	150/50	[3]
MoS_2	2	650	laser	8.44×10^{6}	-	500	[4]
WSe_2/$SnSe_2$	2	532	laser	2×10^{7}	2.15×10^{12}	1×10^{-3}/5×10^{-3}	[5]
Graphene/InSe	1	365	light	1.88×10^{8}	-	22	[6]
WS_2/RGO	-	808	laser	6×10^{3}	-	3.6×10^{4}/5.4×10^{4}	[7]
$PtTe_2$	-	808	laser	600	2.1×10^{8}	340/380	[8]
ReS_2/$PdSe_2$	-	638	laser	5.32×10^{5}	-	7.9×10^{-3}/8.7×10^{-3}	[9]
$ReSe_2$/AZO	0.1	365	laser	150	2.4×10^{10}	-	[10]
Nb_3Cl_8	3	400	light	156.82	4.7×10^{9}	1.45 /1.40	this work

Reference

1. F. Liu, X. Lin, Y. Yan, X. Gan, Y. Cheng and X. Luo, *Nano Letters*, 2023, **23**, 11645–11654.
2. J. Wang, H. Wang, Q. Chen, L. Qi, Z. Zheng, N. Huo, W. Gao, X. Wang and J. Li, *Applied Physics Letters*.
3. X. Wang, D. Pan, M. Sun, F. Lyu, J. Zhao and Q. Chen, *ACS Applied Materials & Interfaces*, 2021, **13**, 26187–26195.
4. Y. Sun, Y. Wang, Z. Wang, L. Jiang, Z. Hou, L. Dai, J. Zhao, Y. Xie, L. Zhao and Z. Jiang, *Advanced Functional Materials*, 2024, 2402185.
5. S. Ghosh, A. Varghese, H. Jawa, Y. Yin, N. V Medhekar and S. Lodha, *ACS nano*, 2022, **16**, 4578–4587.
6. B. Cui, Y. Xing, K. Niu, J. Han, H. Ma, W. Lv, T. Lei, B. Wang and Z. Zeng, *Journal of Science: Advanced Materials and Devices*, 2022, **7**, 100484.
7. S. Ratha, A. J. Simbeck, D. J. Late, S. K. Nayak and C. S. Rout, *Applied Physics Letters*.
8. H. Zhang, L. Du, X. Zhong, W. Wu, Z. Fu, W. Sun, J. Liu, X. Song, J. Zhang and Z. Dai, *Sensors and Actuators A: Physical*, 2024, **371**, 115324.
9. P. Li, Y. Sun, X. Gao, Y. Meng, J. Ma, J. Wang, H. Gao, C. Du, W. Wang and K. Li, *Materials Today Communications*, 2024, **40**, 109945.
10. J. Guo, W. Lei, Y. Zhao, Z. Tan and W. Xie.